Rev. Roum. Sci. Techn.– Électrotechn. et Énerg.
Vol. **71**, *3*, pp. 373–378, Bucarest, 2026

ASYMMETRIC ROTOR TOPOLOGY FOR A SIX-PHASE PERMANENT MAGNET-ASSISTED SYNCHRONOUS RELUCTANCE MOTOR

AMIR HOSEIN AMIRI[1], SEYED EHSAN ABDOLLAHI[1], SAEED HASANZADEH [2]

Keywords: Synchronous reluctance; Optimization; Ferrite magnet; Asymmetric design.

Permanent magnet–assisted synchronous reluctance motors (PMa-SynRMs) are promising for electric vehicles due to high torque density and lower magnet use, yet torque ripple remains a challenge. This paper presents the design and optimization of a six-phase PMa-SynRM to minimize torque ripple while preserving average torque and back-EMF quality. Key rotor parameters, slot pitch, barrier-end geometry, insulation ratio, and magnet width are optimized via the Taguchi method. Performance is evaluated using finite element analysis (FEM). The optimized design significantly reduces torque ripple, maintains average torque, and improves the back-EMF harmonic profile. Thermal analysis confirms safe operation of magnets and windings under rated conditions. The results demonstrate that the proposed approach effectively enhances electromagnetic performance while ensuring thermal reliability.

1. INTRODUCTION

Synchronous reluctance machines (SynRMs) have gained considerable attention in recent years, particularly for electric vehicle applications, due to their robust rotor structure, high efficiency, and magnet-free operation [1,2]. Despite these advantages, conventional SynRMs suffer from inherent drawbacks such as low power factor and relatively high torque ripple, which limit their applicability in high-performance drive systems [23]. To address the low power factor issue, permanent magnets, typically ferrite magnets, can be embedded within the rotor flux barriers, forming a permanent magnet–assisted synchronous reluctance motor (PMa-SynRM) [4,5]. While this approach improves the electromagnetic torque production and power factor, it may simultaneously exacerbate torque ripple if the rotor geometry is not properly designed [7,8].

Several techniques have been proposed to mitigate torque ripple in SynRMs and PMa-SynRMs. These include modifying the rotor barrier configuration, adopting different stator winding arrangements [7,8], applying rotor skewing [9,10], selecting alternative slot–pole combinations [11,12], and employing advanced control strategies [13,14,17]. Although effective, many of these approaches introduce additional manufacturing complexity, increased cost, or reduced torque density. Since the rotor geometry has a dominant influence on torque production and harmonic behavior, topology modification of the rotor barriers represents one of the most efficient and cost-effective methods for torque ripple reduction. Consequently, optimization-based rotor design has become an essential tool for achieving smooth torque characteristics.

More recently, asymmetric rotor designs have emerged as a promising solution for torque ripple mitigation in reluctance machines [18]. By introducing controlled asymmetry in flux barrier geometry or magnet placement, spatial harmonics can be suppressed, leading to improved torque smoothness without significantly compromising average torque. In parallel, there has been a growing interest in multi-phase machine topologies, which offer advantages such as reduced per-phase current rating, improved fault tolerance, and lower torque ripple through harmonic cancellation mechanisms [19,20]. While multi-phase systems are well established, their application to PM-assisted SynRMs with complex rotor structures remains a relatively unexplored research area [21].

Significant research efforts have been dedicated to minimizing torque ripple in synchronous reluctance machines (SynRMs) and their variants. In [22], the Taguchi method was employed to optimize torque characteristics, utilizing flux barrier widths as optimization parameters; this approach reduced torque ripple by 18.3% while increasing average torque and efficiency by 4.7% and 1.1%, respectively. A novel parametrization method was introduced in [23] to enhance design freedom, utilizing spline and fluid-shaped flux barriers in both SynRM and PMa-SynRM designs, with the latter demonstrating superior performance in torque ripple and average torque. To reduce material cost while maintaining performance, an asymmetric rotor structure employing both ferrite and NdFeB magnets was proposed in [24]; this design achieved equivalent average torque and a wider speed range. A comparative study for electric vehicle applications between a permanent magnet synchronous machine (PMSM) and a PMa-SynRM with identical stators but different rotors found that, after optimization, the PMa-SynRM exhibited a 31% higher torque per volume ratio. The Flux Barriers Shift (FBS) technique was validated in [25] as an effective means for torque ripple minimization in PMa-SynRM. Integrated into a three-step design flowchart, FBS presented a viable alternative to conventional rotor skewing, offering simplified manufacturing and preserving average torque and efficiency, albeit with slightly lower ripple reduction effectiveness; experimental prototype testing confirmed its capability to mitigate torque ripple without the performance penalties associated with skewing. Further advancing drive robustness for safety-critical applications, [26] provided a comprehensive experimental assessment of a triple-redundant 9-phase PMa-SynRM. Testing on a 35 kW prototype demonstrated high performance under normal operation and excellent fault tolerance under open-circuit, short-circuit, and inter-turn fault conditions. Significantly, the drive maintained continuous operation at two-thirds of rated torque under worst-case fault scenarios, validating a cost-effective and practical solution for high-integrity systems.

Despite these advances, there is still a lack of streamlined design studies that combine rotor barrier optimization, PM assistance, and multi-phase winding configurations within a unified framework. In particular, the impact of optimized rotor geometry on torque ripple, back-EMF quality, and thermal behavior in multi-phase PMa-SynRMs requires further investigation.

In this paper, a six-phase PM-assisted synchronous reluctance motor is designed and optimized using the Taguchi design of experiments (DOE) method. The novelty lies in introducing an

[1] Electrical and Computer Engineering Department, Babol Noshirvani University of Technology, Babol, Iran.
[2] Electrical and Computer Engineering Department, Qom University of Technology, Qom, Iran.
Emails: amirhosein.amirii@yahoo.com, e.abdollahi@nit.ac.ir, hasanzadeh@qut.ac.ir

DOI: 10.59277/RRST-EE.2026.3.6

asymmetric barrier-end modification, optimized via the Taguchi method, for a six-phase PMa-SynRM, thereby reducing torque ripple and improving THD without increasing machine complexity. Key rotor parameters, including rotor slot pitch, barrier-end geometry, insulation ratio, and magnet width, are systematically evaluated to minimize torque ripple while maintaining average torque and back-EMF quality. Two-dimensional finite element method (FEM) simulations are employed to assess electromagnetic performance, followed by a thermal analysis to verify safe operation under rated conditions. The proposed approach provides an efficient and practical design framework for high-performance PMa-SynRMs intended for electric vehicle applications.

The remainder of this paper is organized as follows. Section 2 presents the initial motor design. Section 3 describes the PM-assisted rotor configuration. Section 4 outlines the Taguchi optimization procedure. Section 5 discusses the optimization results. Section 6 presents the thermal analysis of the optimized design.

2. MACHINE DESIGN AND PM-ASSISTED ROTOR CONFIGURATION

The initial design of the proposed six-phase ferrite-assisted synchronous reluctance motor is derived from classical sizing equations. Using an average air-gap flux density and linear current density (A) for a 1 hp, 1500 rpm, 4-pole machine supplied from a 400 V DC-link, the required D^2L product was calculated. A standard stator frame of 140 mm was specified. Assuming a near-unity aspect ratio *($L/D \approx 1$)* common for 4-pole machines, the resulting air-gap diameter (D) and stack length (L) were determined,

$$P_{out}=\mathrm{C_{mec}}\mathrm{D}^2\mathrm{L}\mathrm{n}B_{ave}A_{lin}. \quad (1)$$

Here, P_{out} is the mechanical output power, C_{mec} is the machine constant, D is the bore diameter, L is the stack length, n is the speed in rps, B_{ave} is the average air-gap flux density, and A_{lin} is the linear current loading. The specific geometry of the rotor barriers will be detailed in a subsequent section. Based on these parameters, the initial torque is estimated as follows:

$$T=\frac{P_{out}}{\omega_b}. \quad (2)$$

The final torque will differ from this initial estimate, as both the detailed rotor geometry and magnet placement influence the output. The next design stage calculates the airgap length using the following empirical ratio standard for small motors,

$$\delta=(0.2\%-0.5\%)D. \quad (3)$$

The airgap length (δ) is determined by both electromagnetic and mechanical constraints. For this design, a slot-per-pole-per-phase value of q = 1 was chosen. Consequently, the total number of slots is derived from the following relationship,

$$S=2pmq, \quad (4)$$

where p is the number of pole pairs, m is the number of phases, and S is the total number of slots. The turns per phase can then be calculated after determining the flux per pole using the following equations,

$$\varphi_\mathrm{p}=B_{ave}\tau_p L, \quad (5)$$

$$\tau_p=\frac{\pi\mathrm{D}}{2p}, \quad (6)$$

where B_{ave} is the average flux density, φ_p is the magnetic flux per pole, τ_p is the pole pitch, p is the number of pole pairs, and L is the stack length; the flux per pole is calculated. To calculate the number of turns, there is:

$$E_{ph,peak}=\omega_\mathrm{b}N_{ph}k_w\varphi_\mathrm{p}=2\pi\mathrm{f}N_{ph}k_w\varphi_\mathrm{p}\leq\mathrm{V_{ph,peak}} \quad (7)$$

Here, f is the electrical frequency, N_{ph} is the number of turns per phase, k_w is the winding coefficient, and φ_p is the flux per pole. With these parameters established, the stator geometry can be detailed. Based on the calculated flux per pole and the derived flux per tooth, and assuming a target tooth flux density, the required tooth width is given by:

$$\varphi_t=\frac{\varphi_p}{\text{number of teeth per pole}}, \quad (8)$$

$$\text{tooth width}=\frac{\varphi_t}{B_t L}, \quad (9)$$

where φ_t is the flux per stator tooth and B_t is the allowable flux density in the stator tooth. The yoke length is derived from the yoke flux, which constitutes half of the total flux per pole. Using an assumed target flux density for the yoke material, its required length is calculated by the following relationship:

$$\text{yoke}=\frac{\varphi_t}{\mathrm{B_y L}}, \quad (10)$$

where B_y is the allowable flux density in the stator yoke. The stator outer diameter is fixed at 140 mm by the existing frame, which also determines the tooth length. The rotor barrier configuration follows the methodology established in [23,24], using a topology with equal rotor slot pitch. The final SynRM design is shown in Fig. 1. The motor characteristics are listed in Table 1.

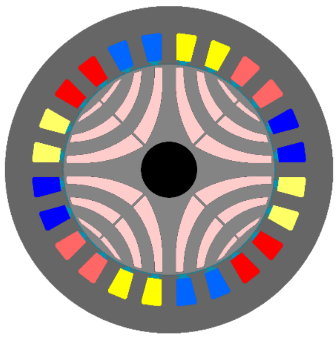

Fig. 1-The initially designed SynRM.

Table 1

Characteristic of the motor

Parameters	Quantity
Rated power	1 *(hp)*
Number of phases	6
Air-gap	0.5 *(mm)*
Rotor diameter	90 *(mm)*
Stack length	90 *(mm)*
Stator outer diameter	140 *(mm)*
Stator bore diameter	91 *(mm)*
Stator tooth width	6.12 *(mm)*
Stator tooth depth (radial)	11.2 *(mm)*
Stator yoke depth	12.36 *(mm)*
Slot opening	2.5 *(mm)*
Rated speed	1500 *(rpm)*
Number of turns per slot	55
Rated RMS current	4.11 *(A)*
Number of slots	24

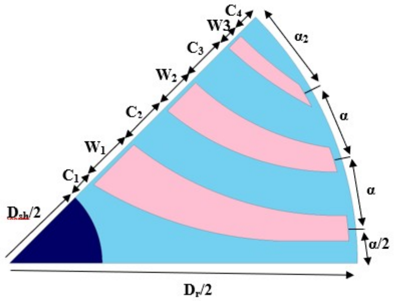

Fig. 2 – The initial rotor design with equal rotor slot pitch *α*.

Figure 2 shows the rotor configuration for the SynRM barriers. The rotor slot pitch for the designed SynRM is calculated as α =11.3 degrees. α_2 is related to *α* by eq.(11) from [23,28]. It is shown in Fig. 2, which is for the third barrier,

$$\alpha_2 = \frac{\pi}{2p} - \alpha(N_b - 0.5), \tag{11}$$

where *p* is the number of pole pairs, and N_b is the number of barriers.

The baseline design is a 1 hp, 4-pole synchronous reluctance motor. Ferrite magnets are integrated into the rotor flux barriers, while the rotor insulation ratio, defined as the ratio between the total barrier width and the total flux carrier (k_{ins}), is maintained,

$$k_{ins} = \frac{\sum_{i=1}^{N_b} W_{bi}}{\sum_{i=1}^{N_b+1} C_i}, \tag{12}$$

Here, N_b is the number of flux barriers, W_{bi} is the width of the i-th barrier, and C_i is the width of the *i*-th flux carrier, as illustrated in Fig. 2.

With the ferrite magnets inserted, the simulated motor achieves an average torque of 7.30 N·m and a torque ripple of 9.58%. The final PM-assisted SynRM design is presented in Fig. 3, while Fig.4 displays its magnetic flux distribution under load.

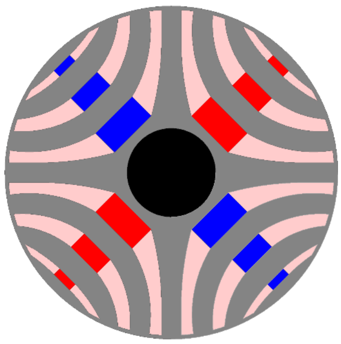

Fig. 3 – The initial PM-assisted rotor design after insertion of magnets.

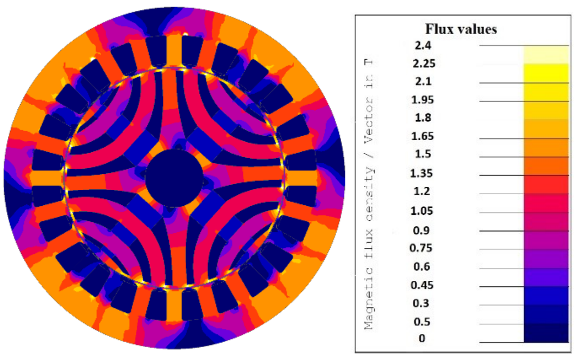

Fig. 4 – Magnetic flux distribution from the 2D FEM simulation of the initial design, operating at 1500 rpm with a phase current of 4.11 A RMS.

3. ROTOR OPTIMIZATION USING THE TAGUCHI METHOD

To efficiently optimize the rotor geometry with a limited number of finite-element simulations, the Taguchi design of experiments (DOE) method is employed. This approach enables the identification of the most influential design parameters while significantly reducing computational cost [29]. Four rotor-related parameters are selected as optimization variables: rotor slot pitch, barrier-end geometry, insulation ratio, and permanent magnet width, also mentioned as *A, B, C,* and *D,* respectively. Each parameter is assigned four discrete levels based on electromagnetic feasibility and manufacturing constraints. Table 2 lists the parameters and their levels.

Table 2

Design Variables and their levels.

Levels	Parameters			
	Rotor slot pitch (*A*)	Barrier end (*B*)	Insulation ratio (*C*)	Magnet width (*D*)
Level 1	11	0.5	0.4	4
Level 2	11.4	1	0.6	6
Level 3	11.8	1.5	0.8	8
Level 4	12.2	2	1	10

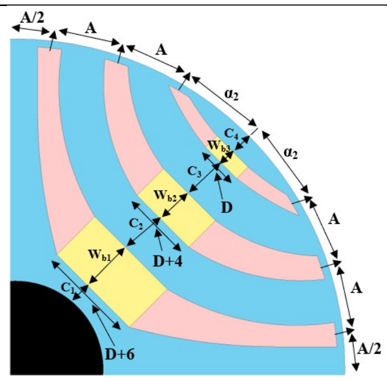

Fig. 5 – Parameters of the rotor geometry.

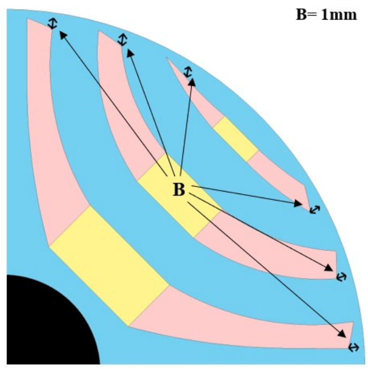

Fig. 6 – Barriers' end modification with parameter B.

The defined parameters are illustrated in Fig. 5. The first parameter is the rotor slot pitch (*A*), α. This pitch remains constant across all flux barriers except for the barrier near the airgap, where a distinct pitch, α_2, is defined by its relationship to α in eq. (10). The second parameter, shown in Fig. 6, modifies the barrier end (*B*) to create an asymmetric rotor shape.

The third parameter is the insulation ratio (*C*), defined by eq. (12) using the dimensions W_{bi} and C_i from Fig. 5, which are the thicknesses of the flux barriers and flux carriers. The fourth and final design variable is the width of the ferrite magnet (*D*). The widths of the two other magnets are *D+2* and *D*+4*,* shown in Fig. 5.

Table 3

Orthogonal array.

Tests	Levels of design parameter			
	Rotor slot pitch(A)	Barrier end(B)	Insulation ratio(C)	Magnet width(D)
1	1	1	1	1
2	1	2	2	2
3	1	3	3	3
4	1	4	4	4
5	2	1	2	3
6	2	2	1	4
7	2	3	4	1
8	2	4	3	2
9	3	1	3	4
10	3	2	4	3
11	3	3	1	2
12	3	4	2	1
13	4	1	4	2
14	4	2	3	1
15	4	3	2	4
16	4	4	1	3

An orthogonal array shown in Table 3 is used to systematically evaluate the impact of the selected parameters on the objective functions, including torque ripple, average torque, fundamental back-EMF amplitude, and total harmonic distortion (THD) of the back-EMF.

Table 4

Experiment results.

Tests	Average torque (N·m)	Torque ripple(%)	V_1 (V)	THD (%)
1	6.88	9.88	3	26.7
2	7.06	6.65	4.20	26.9
3	7.27	8.80	5.71	23.90
4	7.45	12.21	7.39	19.82
5	7.33	7.23	6.18	23.4
6	7.26	8.81	7.40	17.74
7	6.95	8.05	2.77	26.71
8	7.04	8.66	4.07	28.29
9	7.56	6.87	8.16	18.44
10	7.35	9.25	5.98	23.67
11	6.89	6.24	3.98	26.05
12	6.78	9.58	2.65	26.4
13	7.27	13.61	4.70	26.76
14	6.95	12.51	2.88	26.53
15	7.38	6.77	7.47	17.74
16	7.30	11.64	5.76	23.03
Mean value	7.17	9.17	5.14	23.88

The results of the experiments are presented in Table 4. Statistical analysis was performed using Analysis of Means (ANOM), after which the average of each objective function at each level was calculated. The results of the ANOMs are shown in Figs. 7-10.

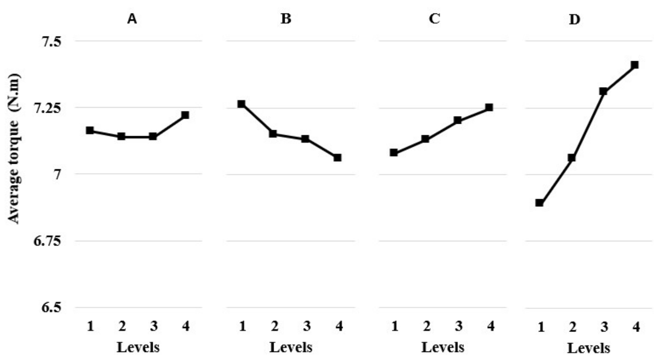

Fig. 7 – Analysis of the mean of the average torque.

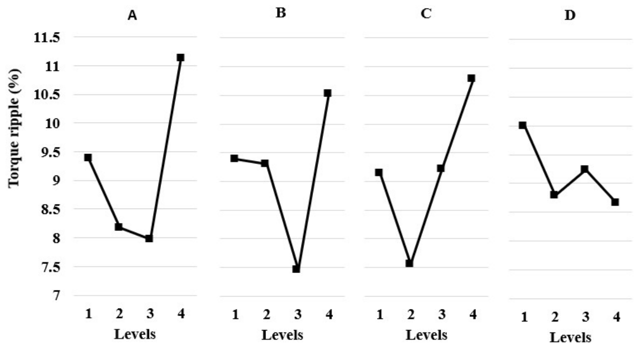

Fig. 8 – Analysis of the mean of the torque ripple.

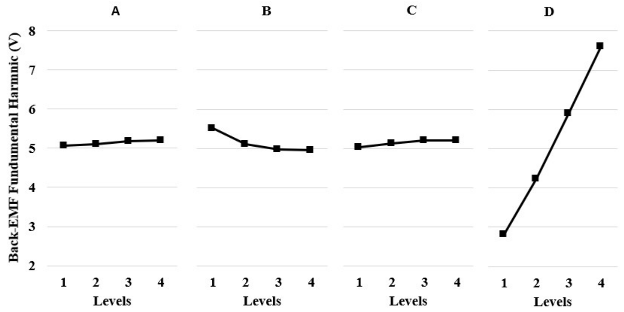

Fig. 9 – Analysis of the mean of the fundamental harmonic order of the back-EMF.

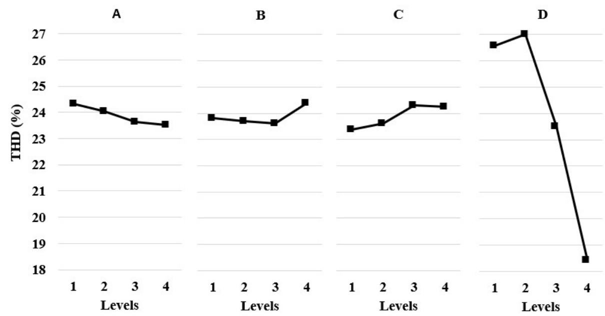

Fig. 10 – Analysis of the mean of THD.

Table 5

Ratio of the effect of each parameter on each objective function.

Objective function	Variable			
	Rotor slot pitch(A)	Barrier end(B)	Insulation ratio(C)	Magnet width(D)
Average torque	2.2 %	5.92 %	8.45 %	83.43 %
Torque ripple	36.1 %	27.63 %	30 %	6.30 %
V_1	0.09%	1.49 %	0.16 %	97.17 %
THD	0.86 %	0.74 %	1.28 %	97.1 %

Analysis of variance (ANOVA), a statistical method, is used to determine the effect of each parameter on each objective function. The ratio of the effect of each parameter on each objective function is calculated for each design case in Table 5 to assess the sensitivity of the objective functions to parameter variations. Based on the variance contribution analysis, magnet width and rotor slot pitch are identified as the dominant parameters influencing the average torque and torque ripple, respectively, while the barrier-end geometry plays a key role in harmonic suppression.

The optimal parameter combination is selected based on the ratio of the parameter effects on the objective function and is subsequently validated through detailed FEM simulations. This optimization framework provides a systematic, computationally efficient approach to improve the torque characteristics of PM-assisted SynRMs.

4. OPTIMIZATION RESULTS AND DISCUSSION

The electromagnetic performance of the optimized PM-assisted SynRM is evaluated through two-dimensional FEM simulations and compared with the initial design. The optimized design is depicted in Fig.11. Table 6 lists the selected levels and their quantities.

Table 6

Selected parameters and their levels after optimization.

Parameter	Rotor slot pitch (A)	Barrier end (B)	Insulation ratio (C)	Magnet width (D)
level	3	3	2	4
Quantity	11.8	1.5	0.6	10
Initial design	12.2	0	0.8	6

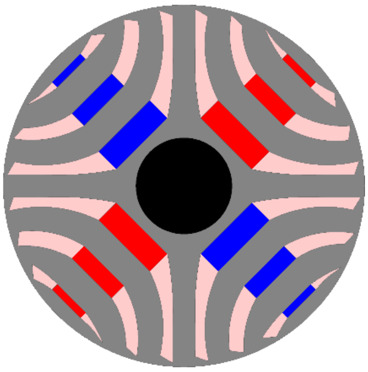

Fig. 11 – Optimized PM-assisted rotor.

As displayed in Fig. 12, the optimized rotor configuration exhibits a notable improvement in torque smoothness, with torque ripple reduced from 9.58% in the initial design to 6.50%, corresponding to a reduction of approximately 32%. At the same time, the average torque is maintained with a slight increase from 7.30 N·m to 7.38 N·m, demonstrating the effectiveness of the optimization strategy.

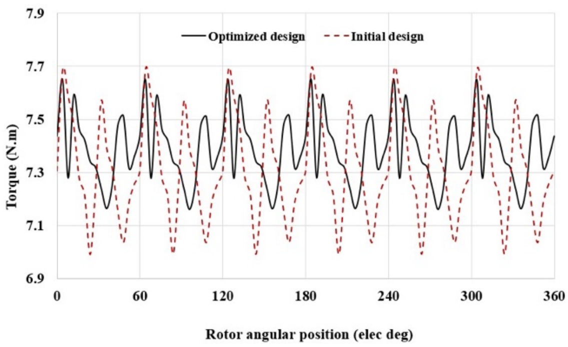

Fig. 12 – Average torque for the initial and optimized design at RMS current of 4.11 A and speed of 1500 rpm.

In addition to torque improvement, the back-EMF waveform shown in Fig.13 exhibits a more sinusoidal behavior after optimization. The harmonic spectra of the back-EMF for both the initial and optimized designs are presented in Fig.14. It can be observed that the fundamental component (1st harmonic) increases, while the dominant low-order harmonics, particularly the 3rd and 5th components, are significantly reduced. The total harmonic distortion (THD), calculated as:

$$\text{THD}=\frac{\sqrt{\sum_{n=2}^{\infty} V_n^2}}{V_1}, \tag{13}$$

where V_n is the harmonic order of the back-EMF. As a result, THD is reduced by 27.26%. The improvement is mainly attributed to enhanced fundamental components and suppressed spatial harmonic components, resulting from optimized rotor slot pitch and refined barrier-end geometry that mitigate local flux saturation effects.

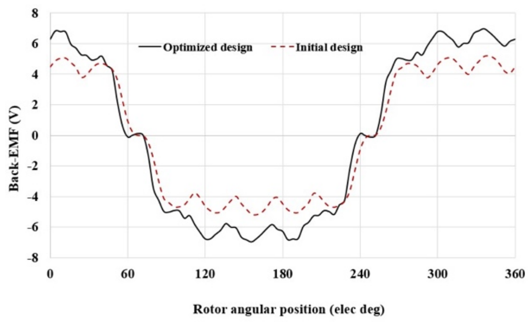

Fig. 13 – Back-EMF of the optimized and initial design.

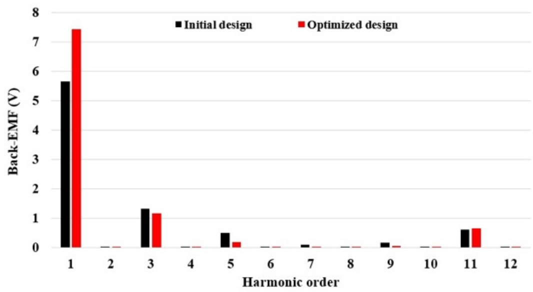

Fig. 14 – Harmonic order of the Back-EMF of the optimized and initial design.

Overall, the optimized PM-assisted SynRM demonstrates balanced improvements in torque quality and electromagnetic performance without compromising average torque output.

5. THERMAL ANALYSIS

Although electromagnetic optimization achieves target performance metrics like torque ripple, the use of permanent magnets in the rotor necessitates a thermal assessment for long-term reliability. This evaluation is particularly critical given the absence of an active cooling system, relying instead on natural convection and radiation. The primary heat sources were calculated analytically: core losses, separated into rotor (1.34 *W*) and stator (10.26 *W*) components using the Bertotti method, and total copper losses of approximately 48 *W*. To prevent irreversible magnet demagnetization and insulation degradation from overheating, a thermal analysis was conducted to confirm safe operating limits under these loss conditions.

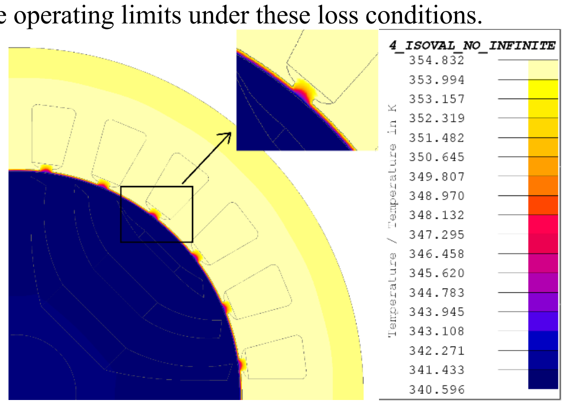

Fig. 15 – Temperature distribution of the optimized design.

As shown in Fig. 15, the permanent magnets reach approximately 340°K (67°C) and the stator windings 354°K (81°C), both within safe limits. These results confirm that the proposed design maintains thermal performance comparable to a conventional synchronous reluctance motor.

6. CONCLUSIONS

In this paper, a PM-assisted synchronous reluctance motor is designed and optimized using the Taguchi design of experiment method with the objective of reducing torque ripple while maintaining key performance indices. The effects of rotor slot pitch, barrier-end geometry, insulation ratio, and magnet width are systematically investigated using finite element analysis. The optimized rotor configuration achieves a substantial reduction in torque ripple with minimal impact on average torque and improved back-EMF harmonic quality. Thermal analysis confirms that the permanent magnets and stator windings operate within safe temperature limits under rated conditions. The proposed asymmetric rotor topology demonstrates that minor geometric modification combined with statistical optimization can significantly improve torque ripple and harmonic performance in six-phase PMa-SynRM without structural complexity increase, making the design suitable for electric vehicle applications.

CREDIT AUTHORSHIP CONTRIBUTION STATEMENT

AMİR HOSEİN AMİRİ: concept, design, data collection and/or processing, analysis and/or interpretation, literature search, writing manuscript.
SEYED EHSAN ABDOLLAHİ: concept, supervision, resources, materials, critical review.
SAEED HASANZADEH: supervision, critical review.

Received on 22 December 2025

REFERENCES

1. N. Bianchi, E. Fornasiero, M. Ferrari, M. Castiello, "Experimental comparison of PM-assisted synchronous reluctance motors." IEEE Transactions on Industry Applications, **52**, *1*, pp. 163–171 (2015).
2. D. Benoudjit, S. Rid, N. Nait-Said, M. Saidnait-Said, L. Chrifi-Alaoui, "Electric vehicle propelled by dual-induction motors structure: Experimental results." Rev. Roum. Sci. Techn. – Électrotechn. et Énerg., **68**, *2*, pp. 170–175 (2023).
3. M. Al-ani, A. Walker, G. Vakil, D. Gerada, C. Gerada, K. Paciura, "Modifications to PM-assisted synchronous reluctance machine to achieve rare-earth-free heavy-duty traction." IEEE Journal of Emerging and Selected Topics in Power Electronics, **11**, *2*, pp. 2029–2038 (2022).
4. W. Chen, Y. Wang, X. Liu, Y. Shi, Y. Zhao, R. Qu, "Comparative study of hybrid PM-assisted synchronous reluctance machines with different configurations." IEEE Transactions on Industry Applications, pp. 1–10 (2025).
5. S. Jani, J. Jamnani, "Performance validation of PM-assisted SynRM and PMSM with optimized design for EV application." Transactions on Energy Systems and Engineering Applications, **4**, *2*, pp. 1–14 (2023).
6. P. Kumar, R. Wilson, A. EL-Refaie, "Electromagnetic design optimization integrated with mechanical stress analysis of PM-assisted synchronous reluctance machine topologies enabled with a blend of magnets." Energies, **17**, *8*, pp. 1873 (2024).
7. A. Nobahari, A. Vahedi, R. Nasiri-Zarandi, "A modified permanent magnet-assisted synchronous reluctance motor design for torque characteristics improvement." IEEE Transactions on Energy Conversion, **37**, *2*, pp. 989–998 (2021).
8. T. Tudorache, "Finite element analysis of a flexible dual-speed salient pole synchronous machine." Rev. Roum. Sci. Techn. – Électrotechn. et Énerg., **70**, *1*, pp. 21–26 (2025).
9. X. Ma, G. Li, Z. Zhu, G.W. Jewell, J. Green, "Investigation on synchronous reluctance machines with different rotor topologies and winding configurations." IET Electric Power Applications, **12**, *1*, pp. 45–53 (2018).
10. B. Lehner, D. Gerling, "Design and comparison of concentrated and distributed winding synchronous reluctance machines." 2016 IEEE Energy Conversion Congress and Exposition (ECCE), pp. 1–8 (2016).
11. P. Lazari, J. Wang, B. Sen, "3-D effects of rotor step-skews in permanent magnet-assisted synchronous reluctance machines." IEEE Transactions on Magnetics, **51**, *11*, pp. 1–4 (2015).
12. R. Tsunata, M. Takemoto, "Skewing technology for permanent magnet synchronous motors: A comprehensive review and recent trends." IEEE Open Journal of the Industrial Electronics Society, pp. 1–10 (2024).
13. S.M. Taghavi Araghi, A. Kiyoumarsi, B. Mirzaeian Dehkordi, "Design, analysis, and prototyping of a PM-assisted synchronous reluctance machine equipped with a new type of fractional-slot winding." IET Electric Power Applications, **19**, *1*, pp. e70002 (2025).
14. F. Li, K. Wang, P. Gao, S. Zhu, C. Liu, R. Jiang, "Investigation of cogging torque and torque ripple in consequent-pole permanent magnet machine with different slot/pole number combinations." Proceedings of the CSEE, **42**, *17*, pp. 6491–6498 (2021).
15. R. Thike, P. Pillay, "Automated current control method for flux-linkage measurement of synchronous reluctance machines." IEEE Transactions on Industry Applications, **56**, *2*, pp. 1464–1474 (2020).
16. X. Sun, Y. Xiong, J. Yang, X. Tian, "Torque ripple reduction for a 12/8 switched reluctance motor based on a novel sliding mode control strategy." IEEE Transactions on Transportation Electrification, **9**, *1*, pp. 359–369 (2022).
17. S. Benaicha, "Robust sensorless speed control of an induction motor drive using a synergetic approach." Rev. Roum. Sci. Techn. – Électrotechn. et Énerg., **68**, *4*, pp. 381–387 (2023).
18. Y. Zheng et al. "A torque ripple reduction method for the synchronous reluctance machines with mirror asymmetric rotor laminations." IEEE Transactions on Industrial Electronics, pp. 1–10 (2025).
19. A.G. Yepes, O. Lopez, I. Gonzalez-Prieto, M.J. Duran, J. Doval-Gandoy, "A comprehensive survey on fault tolerance in multiphase AC drives, part 1: General overview considering multiple fault types." Machines, **10**, *3*, pp. 208 (2022).
20. M. Abdelwanis, R. El-Sehiemy, "Efficient parameter estimation procedure using sunflower optimization algorithm for six-phase induction motor." Rev. Roum. Sci. Techn. – Électrotechn. et Énerg., **67**, *3*, pp. 259–264 (2022).
21. M. Zhao, G. Liu, Q. Chen, W. Zhao, C.H.T. Lee, "Fault-tolerant control of a triple redundant PMA-SynRM driven under single-phase open-circuit by mono-inverter." IEEE Transactions on Power Electronics, **36**, *10*, pp. 11593–11605 (2021).
22. M. Naseh, S. Hasanzadeh, S.M. Dehghan, H. Rezaei, A.S. Al-Sumaiti, "Optimized design of rotor barriers in PM-assisted synchronous reluctance machines with Taguchi method." IEEE Access, **10**, pp. 38165–38173 (2022).
23. O. Korman, M. Di Nardo, M. Degano, C. Gerada, "A novel flux barrier parametrization for synchronous reluctance machines." IEEE Transactions on Energy Conversion, **37**, *1*, pp. 675–684 (2021).
24. Y. Xie, J. Shao, S. He, B. Ye, F. Yang, L. Wang, "Novel PM-assisted synchronous reluctance machines using asymmetrical rotor configuration." IEEE Access, **10**, pp. 79564–79573 (2022).
25. S. Ferrari, E. Armando, G. Pellegrino, "Torque ripple minimization of PM-assisted synchronous reluctance machines via asymmetric rotor poles." 2019 IEEE Energy Conversion Congress and Exposition (ECCE), pp. 4895–4902 (2019).
26. B. Wang, J. Wang, A. Griffo, B. Sen, "Experimental assessments of a triple redundant nine-phase fault-tolerant PMA-SynRM drive." IEEE Transactions on Industrial Electronics, **66**, *1*, pp. 772–783 (2017).
27. R. Rajabi Moghaddam, "Synchronous reluctance machine (SynRM) in variable speed drives (VSD) applications." PhD Thesis, KTH Royal Institute of Technology, Stockholm, Sweden, pp. 1–200 (2011).
28. R. Rouhani, S.E. Abdollahi, S.A. Gholamian, "A simple analytical method for rotor design of synchronous reluctance machines." 2022 13th Power Electronics, Drive Systems, and Technologies Conference (PEDSTC), pp. 420–425 (2022).
29. S.A. Mirnikjoo, K. Abbaszadeh, S.E. Abdollahi, "Multiobjective design optimization of a double-sided flux-switching permanent magnet generator for counter-rotating wind turbine applications." IEEE Transactions on Industrial Electronics, **68**, *8*, pp. 6640–6649 (2020).